Science of the Total Environment 771 (2021) 144811

Contents lists available at ScienceDirect

Science of the Total Environment

journal homepage: www.elsevier.com/locate/scitotenv

Optimized remote sensing estimation of the lake algal biomass by considering the vertically heterogeneous chlorophyll distribution: Study case in Lake Chaohu of China

Minqi Hu [a,b], Yuchao Zhang [a,*], Ronghua Ma [a,c], Kun Xue [a], Zhigang Cao [a,b], Qiao Chu [a,b], Yuanyuan Jing [a,b]

[a] Key Laboratory of Watershed Geographic Sciences, Nanjing Institute of Geography and Limnology, Chinese Academy of Sciences, Nanjing 210008, China
[b] University of Chinese Academy of Sciences, Beijing 100049, China
[c] Lake-Watershed Science Data Center, National Earth System Science Data Center, National Science & Technology Infrastructure of China, China

HIGHLIGHTS

- A novel algorithm is proposed to estimate algal biomass.
- The entire unit column biomass of algae in Lake Chaohu is estimated.
- ABI is relatively insensitive to atmospheric conditions and suspended matter.
- We evaluate the applicability to other remote sensors.

GRAPHICAL ABSTRACT

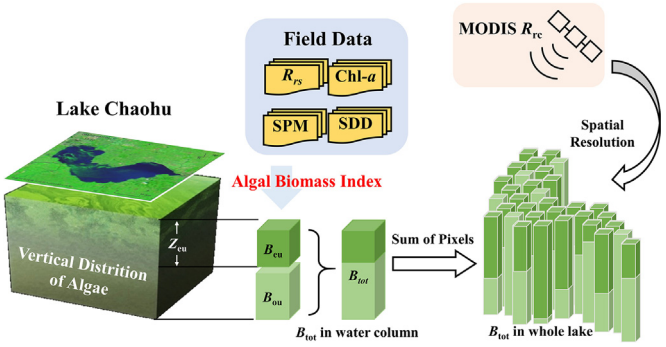

ARTICLE INFO

Article history:
Received 2 October 2020
Received in revised form 21 December 2020
Accepted 22 December 2020
Available online 27 January 2021

Editor: Ashantha Goonetilleke

Keywords:
Remote sensing
Algal biomass
MODIS
Lake Chaohu
Aerosol

ABSTRACT

Due to the difference of vertical distribution of algae in lakes, it is necessary to carry out remote sensing estimation of algal biomass based on the vertically heterogeneous distribution of chlorophyll in order to improve the accuracy of biomass inversion. A new algorithm is proposed and validated to measure algal biomass in Lake Chaohu based on the Moderate Resolution Imaging Spectrometer (MODIS) images. The algal biomass index (ABI) is defined as the difference in remote-sensing reflectance (R_{rs}, sr^{-1}) at 555 nm normalized against two baselines with one formed linearly between R_{rs}(859) and R_{rs}(469) and another formed linearly between R_{rs}(645) and R_{rs}(469). Both theory and model simulations show that ABI has a good relation with the algal biomass in the euphotic zone ($R^2 = 0.88$, $p < 0.01$, $N = 50$). Field data were further used to estimate the biomass outside the euphotic layer through an empirical algorithm. The ABI algorithm was applied to MODIS Rayleigh-corrected reflectance (R_{rc}) data after testing the sensitivity to sun glint and thickness of aerosols, which showed an acceptable precision (root mean square error < 21.31 mg and mean relative error < 16.08%). Spectral analyses showed that ABI algorithm was immune to concentration of colored dissolved organic matter (CDOM) but relatively sensitive to suspended particulate inorganic matter (SPIM), which can be solved by using Turbid Water Index (TWI) though in such a challenging environment. A long-term (2012–2017) estimation of algal biomass was further calculated based on the robust algorithm, which shows both seasonal and spatial variations in Lake Chaohu. Tests of ABI algorithm on Sentinel-3 OLCI demonstrates the potential for application in other remote sensors, which meets the need of observation using multi-sensor remote sensing in the future.

* Corresponding author.
E-mail address: yczhang@niglas.ac.cn (Y. Zhang).

https://doi.org/10.1016/j.scitotenv.2020.144811
0048-9697/

1. Introduction

Eutrophic lakes have attracted much attention due to the serious decline in water quality and increase of cyanobacterial blooms (Jiang et al. 2014). Satellite observations allow a useful approach to explore the temporal and spatial changes of inland lakes, providing the ability to study eutrophication by determining the frequency and coverage of algal blooms (Kutser et al. 2006; Zhang et al. 2014). When the algae multiply and gather on the surface of inland lakes, the water color appears green and algal blooms are formed (Oliver and Ganf 2007). Many algorithms, such as the floating algae index (FAI) (Hu 2009; Hu et al. 2011), ocean surface algal bloom (Shanmugam et al. 2013), color index (Lee et al. 2012), and maximum peak-height algorithm (Matthews et al. 2012), have been widely used for monitoring algal blooms in inland waters. These algorithms extract important information about the optically active components in surface waters through remotely sensed reflectance (R_{rs}), backscattering and absorption. However, the vertical movement of algae can cause sudden increases in surface chlorophyll *a* (Chl-a) (Cao et al. 2006; Serôdio et al. 2009; Kong and Gao 2005) and lead to inaccurate results in estimation of algal biomass from a single surface value (Lee et al. 2012).

Algal biomass can be estimated based on the relationship between Chl-a concentrations of water surface and phytoplankton biomass in water column (Lwjr et al. 1992) or the retrieval of the vertical concentration in Chl-a. The latter is based on the assumption of a constant Gaussian vertical profile and has been used to estimate the primary production of marine systems (Frolov et al. 2012; Uitz et al. 2006; Silulwane et al. 2001). These estimates are validated to be accurate because of the vertical structure of most marine waters. However, the estimation of algal biomass in inland lakes is more complex than that in oceanic or coastal waters (Binding et al. 2008; Shi et al. 2014). There are several reasons for this:1) lakes of the Yangtze River are mostly shallow lakes and susceptible to wind and waves that cause re-suspension of the sediment, resulting in higher suspended matter concentrations and lower transparency (Shi et al., 2015); 2) hydrodynamic conditions are mainly caused by wind disturbances on the surface of the lake, which cause significant water disturbances on the algal growth, aggregation and distribution (Liang et al. 2013); 3) variation of algal biomass caused by different vertical distribution (Xue et al. 2016). Therefore, algal biomass can be estimated based on two assumptions: 1) homogenous distribution of chlorophyll in the water column (Ma et al. 2014); 2) interpolation from discrete biomass samples based on the water column integrated algal biomass (Li et al. 2017). These assumptions were considered to be applicable for algal biomass estimation under non-algal bloom conditions (Li et al. 2017), algal bloom conditions (Li et al. 2018) or vertical uniformity, which cannot apply to the whole eutrophic lake where regional algal bloom accumulated. In addition, interpretation from separate biomass samples will cause discontinuities in calculated values (Liu and Wan 2018), which does not meet the fact of the continuous spatial distribution of algae in the entire lake and the accuracy of the inversion (Duan et al. 2008).

Vertical inhomogeneity of phytoplankton influences not only the inversion of Chl-a but also analytical models of phytoplankton biomass that require depth-dependent values of Chl-a concentration (Silulwane et al., 2001; Xue et al. 2017). Approaches to estimate algal biomass in different vertical distributions are important to improve the accuracy of algal biomass estimation. The study constructed a method for remote estimation of algal biomass based on vertical Chl-a concentrations and R_{rs}, which was obtained by a field experiment and radiation transmission simulation using Ecolight (Mobley and Sundman 2008). The water column was divided in two parts: in the euphotic zone and outside the euphotic zone. We first established a relationship between the remote sensing reflectance (R_{rs}) and the algal biomass in the euphotic zone (B_{eu}). A new algal biomass index (ABI) was accordingly proposed. Then, algal biomass outside the euphotic depth (B_{ou}) was determined by an empirical algorithm. The study can not only grasp the spatial and temporal distribution of algal biomass, but also provide important support for the estimation of algal biomass in eutrophic lakes.

2. Materials and methods

2.1. Study area

Lake Chaohu (31°25′–31°43′N, 117°17′–117°51′E), located in the middle of Anhui Province (Fig. 1), is the fifth largest freshwater lake in China with an area of 770 km^2. The average depth of Lake Chaohu is 3.0 m and the maximum depth is 6.0 m (Tang et al. 2015; Zhang et al. 2016). Considering that the near-shore area has an impact on the waters, the water boundary is reduced by one pixel to reduce the interference from the near-shore area in this study. The concentration of total

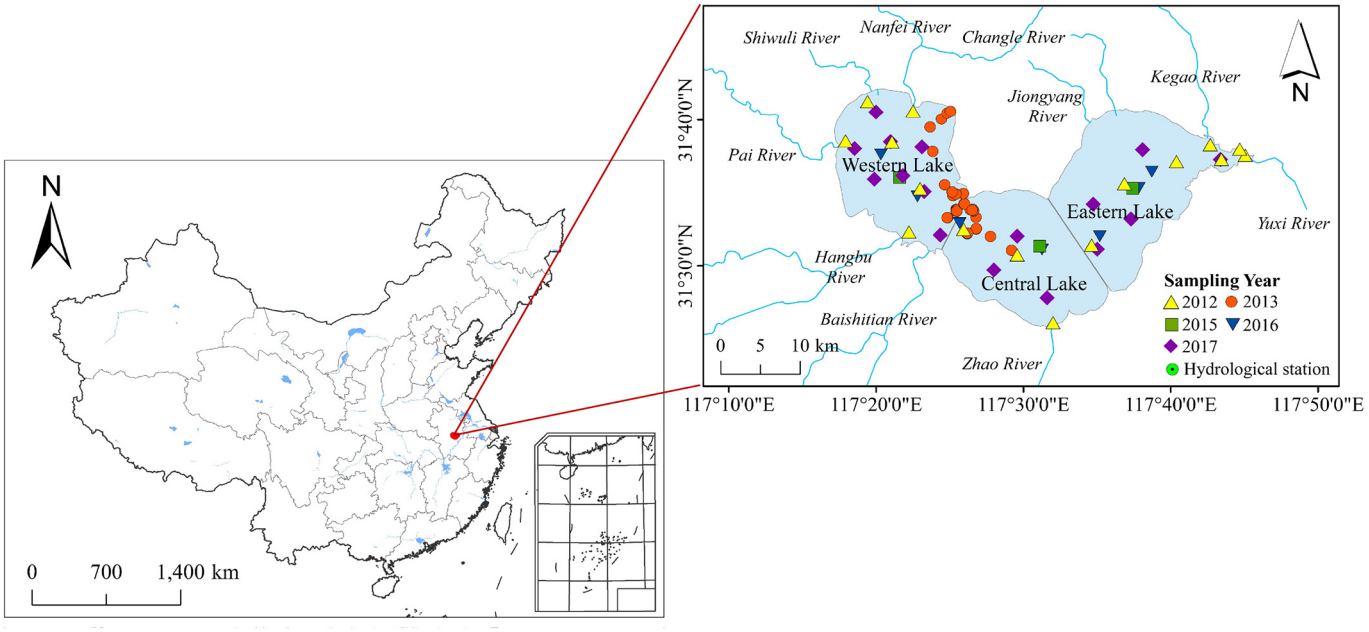

Fig. 1. Location of Lake Chaohu with three segments and distribution of field sample.

phosphorus (TP) in Lake Chaohu is 0.04–1.40 mg/L, with an average of 0.20 mg/L; the concentration of total nitrogen (TN) is 0.84–23.0 mg/L, with an average of 3.85 mg/L (Xi et al. 2016). The mean turbidity (NTU) of Lake Chaohu is 21.05 (Zhang et al. 2016). The location of Chaohu belongs to subtropical monsoon climate that annual average rainfall is 1100 mm and annual average temperature is 15 °C–16 °C (Chen et al. 2013).

With the increase of population, agriculture and the accelerated development of industry in recent years, the aquatic environment has been severely damaged (Wang et al. 2013; Lei et al. 2020a; Lei et al. 2020b). A large number of organisms in the lake have died, and the water quality has deteriorated, seriously threatening the safety of drinking water (Zhang et al. 2015). Algal blooms (primarily *Microcystis* and *Anabaena*) have dominated this lake over the past few decades (Zhang et al. 2016). It has found that Lake Chaohu is dominated by *Anabaena* in spring, *Microcystis* in summer, and it is transformed into *Anabaena* in autumn and winter (Wang et al. 2018). From the perspective of spatial distribution, *Microcystis* is mainly distributed in the Western Lake, *Anabaena* and *Mitomyces* are distributed in the Eastern Lake, *Mitomyces* is distributed in the Central Lake. Therefore, algal blooms represented by *Mitomyces* appeared in the Eastern Lake in winter. In spring, the average temperature is less than 25 °C and algal blooms mainly appeared in the eastern and central lake at the same time. In summer and autumn, *Microcystis* grew and floated, which causes large areas of blooms appear in the Western Lake. After October, the dominant algal species of algae gradually changed through the decreasing temperature. Algal blooms in the West Lake area gradually decreased, and were more concentrated in the Eastern Lake (Hu et al. 2018). The eutrophication in the western part of Lake Chaohu is more serious than that in the central and eastern parts, mainly because river runoff is an important way to transport pollutants to Lake Chaohu (Jiang et al. 2014; Tang et al. 2015).

2.2. Data acquisition

2.2.1. Field data

102 water samples with optical data from Lake Chaohu were collected in May, July, and October of 2013, April of 2015, September and December of 2016, and November of 2017, covering the whole lake (Fig. 1). 50 random-selected samples supported the establishment of algorithm, containing every sampling time. The rest of samples ($N = 52$) were used for independent verification.

Remote sensing reflectance spectra $R_{rs}(\lambda)$ was measured using an ASD handheld spectrometer (FieldSpec Pro Dual VNIR, Analytical Spectral Devices, Inc.) following the NASA Ocean Optics protocols (Mueller et al., 2003), the measurement range is 350-1050 nm with an interval of 1 nm. The total water leaving radiance (L_{sw}), the radiance of reference gray panel reflectance (L_p), and the sky radiance (L_{sky}) were measured to derive the R_{rs} with viewing direction of 45° from the nadir and 135° azimuth with the respect to the sun. The downwelling irradiance ($E_d(\lambda)$), was calculated using measurements of radiance from a 30% reflecting gray reference (ρ_p) (Mobley 1999). The collection device, composed of a graduated profiling sampling wire, a small vacuum pump, a connective tube, and a portable battery (Li et al. 2017), was used to collect water samples at different vertical depths (0, 0.1, 0.3, 0.5, 0.7, 1, 1.5, 2 and 3 m). Considering that wind speed affects the vertical distribution of algae and the vertical heterogeneity of algae occurs under the wind speed that less than 3 m/s (Cao et al. 2006), field experiments were carried out at wind speeds below 3 m/s. Water samples at each site were filtered onboard and then returned to the laboratory. Chl-a ($\mu g \cdot L^{-1}$) were determined using 47 mm Whatman GF/F glass fiber filters and ethanol extraction (Ma et al. 2006). With 0.7 μm GF/F glass fiber filters, water samples were filtered and then heated in an oven for 4–6 h (105 °C), suspended particulate matter (SPM, in $mg \cdot L^{-1}$) were measured using the weighing method (GB11901-89 Standard). These samples were further heated in the oven for 3–4 h (450 °C) to obtain the concentrations of suspended particulate inorganic matter (SPIM, in $mg \cdot L^{-1}$) (Cao et al. 2017).

Algal biomass itself is a poorly defined term, usually in turn estimated by one or more parameters such as dry weight or wet weight, cell volume, particulate carbon or Chl-a (Carlson 1977). However, estimation based on remote sensing is obtained by calculating the weight of Chl-a or the integrated chlorophyll biomass (Morel and Berthon 1989; Li et al., 1995; Ma et al. 2014). At each station, the total algal biomass in unit water column (B_{tot}, mg) was calculated using Chl-a at different vertical water depths as Eq. (1):

$$B_{tot} = \Sigma\{[Chla(Z_{N+1}) + Chla(Z_N)]/(Z_{N+1} - Z_N)\} \times A \quad (1)$$

where Z_N and Z_{N+1} refer to water depth of the Nth and the $(N + 1)$th sample, $0 < N \le 8$ as nine vertical samples were collected at different water depths (0, 0.1, 0.3, 0.5, 0.7, 1, 1.5, 2, and 3 m), A refers unit area and is 1 m^2. Therefore, algal biomass of the whole lake in a remote sensing image can be calculated by multiplying B_{tot} and spatial resolution of sensor with sum of pixels, and using the unit into ton(t) for whole lake statistics as Eq. (2):

$$B_{lake} = \sum_{1}^{N} B_{tot} \times R^2 \quad (2)$$

where R refers to spatial resolution(m) of MODIS and its value is 250, N refers to number of pixels in range of Lake Chaohu.

106 water samples, mentioned in previous Li's study (Li et al. 2017), were obtained to make comparison with previous algorithm. In this dataset, water samples were collected from January 2012 to December 2013 at 16 fixed sites and filtered from three different depths (0.5, 1.5, and 3 m). The measurement of Chl-a and SPIM are the same as those of the above-mentioned samples. These field samples were mixed equally to estimate integrated total algal Chl-a concentration (Li et al. 2017) and used for comparison of precision. The depth of euphotic zone (Z_{eu}) for the measured dataset was calculated using an empirical algorithm, which had proposed for Lake Taihu and confirmed the potential for other turbid eutrophic lakes as Eq. (3) (Le et al. 2008).

$$Z_{eu} = 2.8023e^{-1.9422Rrs(732/532)} \quad (3)$$

2.2.2. Radiative transfer simulation data

The vertical distribution of algae in Lake Chaohu can be divided into four types: uniform type, Gaussian type, exponential type and hyperbolic type (Xue et al. 2015). However, field data cannot encompass all types of the concentration of components and algae distribution. Thus, the radiation transmission model was used to simulate the physical process of light transmission in water, and a large-scale dataset corresponding to the vertical distribution of different algae can be obtained.

A Hydrolight–Ecolight model was used to simulate the $R_{rs}(\lambda)$ of the water by carrying out radiative transfer simulations of the underwater light field, and inherent optical properties (IOPs) are associated with optically active constituents. Common input parameters of Ecolight (V5.3.0.1, *Sequoia Scientific*, *Inc*) simulation for different vertical distribution of algae were listed in *SI Appendix*, Table. S1.

The setting of the boundary conditions included: the distribution of sunlight and sky light incident on the water surface as simulated by a RADTRAN subroutine, and the solar zenith angle was set to 30°, assuming that the sky was clear and cloudless. It was only used to calculate the angle of the incident light caused by the surface roughness of the water body, and does not affect the vertical direction of the water component. The input wind speed was based on the statistical results of the lake meteorological data and set at 2.25 m/s according to the annual mean value. The default refractive index of the water body is 1.34, which is used to calculate the Fresnel reflectivity of the air-water interface (Mobley 1994). Considering the water depth (average 3 m) and

transparency (less than 60 cm) of Lake Chaohu, water information outside the euphotic zone cannot be transmitted to the water surface and acquired by the sensor. Therefore, the water body was assumed to be optically infinitely deep in the simulation process, and the influence of bottom reflection on the remote sensing reflectance was not considered (Lodhi and Rundquist 2001; Ma et al. 2006; Ma et al., 2011a; Ma et al. 2011b). All simulations consider the Raman scattering of water molecules. Different SPIM and $a_g(440)$ corresponding to the reference wavelength of 440 nm were simulated to examine the robust of the algorithm under different optically active substances. More details about input settings of Ecolight simulations see Xue's study (Xue et al. 2017).

The simulated R_{rs} at different vertical distribution and the diffuse attenuation coefficient of the downwelling spectral irradiance at 490 nm (K_d (490)) of different water depth can be obtained through the Ecolight radiation transmission simulation. Previous study has proved a significant positive correlation between K_d (490) and the photosynthetically available radiation (K_d (PAR)) for a similar extremely turbid shallow lake, Lake Taihu ($R^2 = 0.98$, $p < 0.01$, $N = 81$) (Zhang et al. 2012), which was described as Eq. (4):

$$K_d(PAR) = 0.896 \times K_d(490)^{0.873} \tag{4}$$

The depth of euphotic zone (Z_{eu}) can be further calculated as Eq. (5) (Kirk 1994):

$$Z_{eu} = 4.605/K_d(PAR) \tag{5}$$

2.2.3. Satellite data

The MODIS sensor is carried by the Terra satellite and the Aqua satellite in the Earth Observing System (EOS) program. It has 36 spectral channels covering the visible to near infrared (0.4 to 1.4 μm) spectrum. The scanning width is 2300 km, the spatial resolution of the subsatellite point is 250 m, 500 m and 1000 m, which is much better than the 1100 m resolution of NOAA-AVHRR, and the global data is obtained once every 1–2 days. The MODIS 250 m and 500 m bands were originally designed as "sharpening" bands for land studies and cloud detection (Hu et al. 2004). It is necessary to use these bands which have lower sensitivity to inland water, especially turbid water, than that have better application to ocean. At the same time, NASA has implemented a worldwide policy of receiving and using MODIS data for free, which makes it suitable for use. The higher temporal resolution of MODIS data (crossing times of 10:30 am and 1:30 pm in one day) (Tang et al. 2005), the cheap method of data acquisition makes it the best data source for real-time monitoring algal blooms (Kahru 1994), surface oil slicks (Hu 2009) and coastal/estuarine water quality (Miller and Mckee 2004; Petus et al. 2010).

The MODIS Level-0 data from January 2012 to December 2017 were obtained from National Aeronautics and Space Administration (NASA, http://oceancolor.gsfc.nasa.gov). Radiometric calibration was performed using SeaDAS (SeaWiFS Data Analysis System, USA, version 7.4) to obtain L1B data, and the effects of ozone absorption and molecular Rayleigh scattering were removed to obtain MODIS Rayleigh corrected reflectance $R_{rc}(\lambda)$ as Eq. (6) (Le et al. 2013):

$$R_{rc}(\lambda) = \rho_t(\lambda) - \rho_r(\lambda) = \rho_a(\lambda) + \pi \times t(\lambda) \times t_0(\lambda) \times R_{rs}(\lambda) \tag{6}$$

where ρ_t is the top of atmosphere reflectance after the gaseous absorption adjustment, ρ_r is the reflectance due to Rayleigh scattering, ρ_a is scattering and aerosol-Rayleigh interactions that due to aerosol, and t and t_0 are the diffuse transmittance from the water surface to the satellite and from the sun to the water surface, respectively. ρ_a, t, and t_0 are functions of aerosol type, aerosol optical thickness, and solar/viewing geometry. The formula assumes that the contribution of whitecaps and sunlight can be neglected, and was used to show the relationship between R_{rc} and R_{rs} in this study. The R_{rc} data are reprojected to a cylindrical equidistance (rectangular) projection (Feng et al. 2012).

Since MODIS has exceeded its service time, the applicability of algorithm to other satellite data was also explored. The new generation of OLCI carried on the Sentinel-3 satellite has a revisit period less than 3d, high signal-to-noise ratio with 21 bands to meet the needs of continuous observation (Bi et al. 2018), laying a foundation for the long-term observations of the algal biomass. OLCI Level-1B products was downloaded from EUMETSAT (https://archive.eumetsat.int/usc/) and R_{rc} data was obtained after Rayleigh correction using 6SV (Second Simulation of a Satellite Signal in the Solar Spectrum) model. The floating algae index (FAI) (Hu, 2009), based on Rayleigh corrected reflectance, was used to extract algal blooms in Chaohu. Area of algal bloom was calculated based on algae pixel-growing algorithm (APA) (Zhang et al. 2014). Datasets used in the study are summarized in *SI Appendix*, Table. S2.

2.2.4. Hydrological data

Digital elevation model (DEM) data of Lake Chaohu in 2009 with a spatial resolution of 30 m was obtained from Lake-Watershed Science Data Center, National Earth System Science Data Sharing Infrastructure, National Science & Technology Infrastructure of China (http://lake.geodata.cn). Water level data from Zhongmiao hydrological station (see Fig. 1) from 2012 to 2016 (provided by Hydrology Bureau of Anhui Province) were collected. The study assumes that water level of the entire lake is same as that of at Zhongmiao Station, and the water depth (m) were obtained by subtracting the water level from the DEM.

2.3. Methodology

2.3.1. Euphotic biomass estimation based on in situ R_{rs}

The remote sensing reflectance at the surface is dependent on the vertical structure of the optical properties (Zaneveld et al. 2005). In other words, the signals detected by remote sensing include not only the information of the water surface but also the structure of the underwater light field within a certain depth. Different concentrations of Chl-a (Fig. 2(a)) and corresponding R_{rs} curves (Fig. 2(b)) from field data collected on different sampling date (28th of May, 21st of July on 2013, 10th of April on 2015 and 10th of September on 2016) showed variations in the vertical Chl-a concentration, which influenced algal biomass in the euphotic zone (B_{eu}) and changed spectral reflectance. SPM and SPIM of four representative samples were listed in *SI Appendix*, Table S3. Vertically heterogeneous distribution of chlorophyll particularly affects the red and near-infrared (NIR) bands and slightly affects the blue and green bands.

Inspired by the FAI method, which built a baseline to extract algal bloom (Hu 2009), the low saturation bands of MODIS were used in the study to build two baselines. One based on the near infrared (859 nm), blue (469 nm) and green (555 nm) bands and another based on the red (645 nm), blue and green bands. To eliminate the effects of aerosols in the red and near-infrared bands, a formula (ABI_1) was subtracted from another (ABI_2), which can be described as the difference between the peak heights when the green band(555 nm) is calculated by two different baselines. For details the structure of ABI, please refer to *SI Appendix*, Text S1, Fig. S1.

Therefore, the Algal Biomass Index (ABI) is defined as Eqs. (7)–(9):

$$ABI = ABI_1 - ABI_2 \tag{7}$$

$$ABI_1 = (R_{rs,GREEN} - R_{rs,BLUE}) - (R_{rs,NIR} - R_{rs,BLUE}) \times \frac{\lambda_{GREEN} - \lambda_{BLUE}}{\lambda_{NIR} - \lambda_{BLUE}} \tag{8}$$

$$ABI_2 = (R_{rs,GREEN} - R_{rs,BLUE}) - (R_{rs,RED} - R_{rs,BLUE}) \times \frac{\lambda_{GREEN} - \lambda_{BLUE}}{\lambda_{RED} - \lambda_{BLUE}} \tag{9}$$

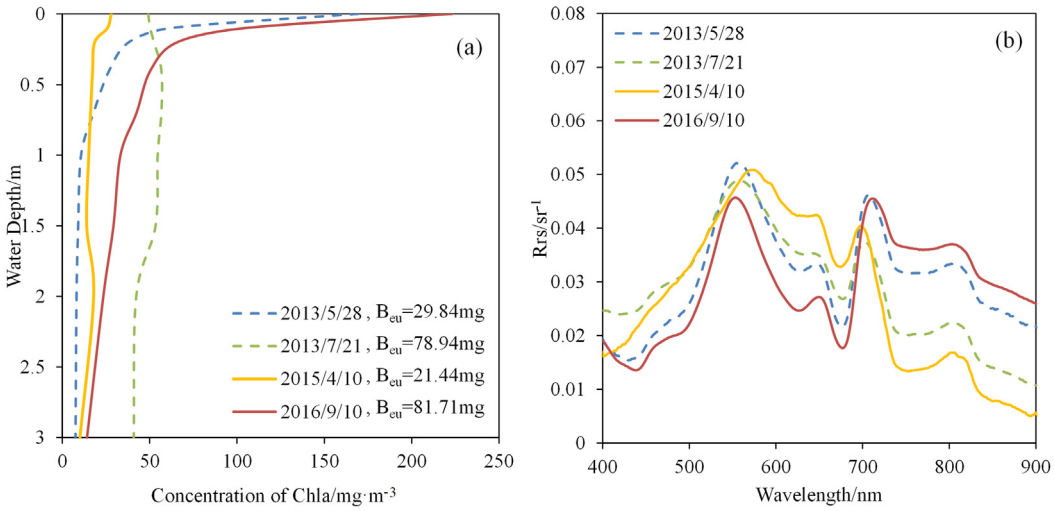

Fig. 2. (a) Vertical Chl-a at different water depths and (b) corresponding R_{rs} curves.

Combining two equations and ABI can be derived as Eq. (10):

$$ABI = (R_{rs,RED} - R_{rs,BLUE}) \times \frac{\lambda_{GREEN} - \lambda_{BLUE}}{\lambda_{RED} - \lambda_{BLUE}} - (R_{rs,NIR} - R_{rs,BLUE}) \times \frac{\lambda_{GREEN} - \lambda_{BLUE}}{\lambda_{NIR} - \lambda_{BLUE}} \quad (10)$$

2.3.2. Biomass outside the euphotic zone

Information of optical properties, observed by remote sensing reflectance ($R_{rs}(\lambda)$) within the penetration depth where the downwelling irradiance (E_d) is reduced to 1/e of its surface value (Gordon and McCluney, 1975; Xue et al. 2017), cannot be detected below the euphotic zone. Therefore, algal biomass outside the euphotic zone (B_{ou}) was indirectly calculated by algal biomass in the euphotic zone (B_{eu}) and an empirical algorithm was established by comparing B_{eu} and B_{ou}. Therefore, B_{tot} can be obtained by adding B_{eu} and B_{ou}. Monthly and yearly algal biomass were calculated through dividing the daily ABI-retrieved algal biomass in whole lake by the number of days in one month or year. The flow chart of algal biomass estimation was shown in *SI Appendix*, Fig. S2.

2.4. Accuracy assessment

Field data and MODIS satellite data were used to verify the accuracy of the algorithm. Two indicators were used: the root mean square error (RMSE) (Mentaschi et al. 2013) and mean relative error (MRE) (Safonov and Chiang 1988). These metrics are defined as Eqs. (11) and (12) separately:

$$RMSE = \sqrt{\frac{1}{N}\sum_{i=1}^{N}(y_i - x_i)^2} \quad (11)$$

$$MRE = \frac{1}{N}\sum_{i=1}^{N}\frac{|y_i - x_i|}{x_i} \quad (12)$$

where x_i is the measured value, y_i is the predicted value of the ith sample, and N is the number of samples.

3. Results

3.1. Construction of model

3.1.1. Estimation of B_{eu}

Relationships between the R_{rs}-based index ABI(R_{rs}) and measured B_{eu} were shown in Fig. 3 (a). The relationship between measured B_{eu} and ABI is consistent with the relationship represented by Gaussian simulated data from Ecolight radiative transfer modelling and $R^2 = 0.88$ ($p < 0.01$, $N = 277$). However, differences in algal bloom formation were found between the non-Gaussian (exponential type and hyperbolic type) simulated data and the measured B_{eu} data. On the one hand, different ranges of SPIM and CDOM concentrations were set for radiative transfer simulations, including boundary cases, not all of which apply to Lake Chaohu; on the other hand, measured Chl-a is a stratified result (from different water depths), which will be discrepancies with the simulated results. However, partial overlap in Fig. 3(a) between the simulated and measured results confirmed the intersection of theory and practice.

Therefore, the measured data and Gaussian simulated data were both used to fit the relationship, and a power function relation was fitted with the measured R_{rs} data and Gaussian type simulated R_{rs} data as Eq. (13):

$$B_{eu} = 96.256 \times (ABI(R_{rs}) + 1)^{-84.96} \quad (13)$$

ABI(R_{rs}) and ABI(R_{rc}) under different observation angles ($\theta_0 = 40°$, $\theta = 20°$, $\Phi = 40°$; $\theta_0 = 40°$, $\theta = 20°$, $\Phi = -120°$; $\theta_0 = 40°$, $\theta = 40°$, $\Phi = 40°$; $\theta_0 = 60°$, $\theta = 20°$, $\Phi = -120°$; $\theta_0 = 60°$, $\theta = 40°$, $\Phi = -120$) for optical thicknesses when $\tau a555 = 0.5$, aerosol type r30f95v01 (Fig. 3(b)), aerosol types (r30f95v01; r50f95v01; r75f95v01; r80f95v01; r85f95v01; r90f95v0) for $\tau a555 = 0.5$, $\theta_0 = 40°$; $\theta = 20°$; $\Phi = 40°$ (Fig. 3(c)) and different aerosol thicknesses of $\tau a555$ (0.1, 0.5, 1.0, 1.5, 2.0) for aerosol type r30f95v01, $\theta_0 = 40°$; $\theta = 20°$; $\Phi = 40°$ (Fig. 3(d)) from SeaDAS LUTs were simulated and compared to explore the algorithm sensitivity to aerosol perturbations. The linear relationship was found between ABI(R_{rs}) and ABI(R_{rc}) ($R^2 = 0.99$, $p < 0.01$, $N = 160$), which illustrates that ABI(R_{rc}) can be calculated by ABI(R_{rs}). That is to say, when remote sensing approaches cannot obtain accurate R_{rs}, R_{rc}-based algorithm can also be used to calculate the total algal biomass as a substitute. Combining all atmospheric conditions and angles of observation, ABI(R_{rc}) was derived as Eq. (14):

$$ABI(R_{rc}) = 3.0665 \times ABI(R_{rs}) - 0.0008 \quad (14)$$

3.1.2. Estimation of B_{ou}

Relationship between B_{eu} and B_{ou} (calculated to 3 m) was shown in *SI Appendix*, Fig. S3. When dramatic changes happened in B_{eu} with 62.91% coefficient of variance (CV), the algal biomass outside the euphotic layer has been affected slightly (CV = 34.60%). Different types of model (linear, exponential or quadratic linear model) were used to describe the

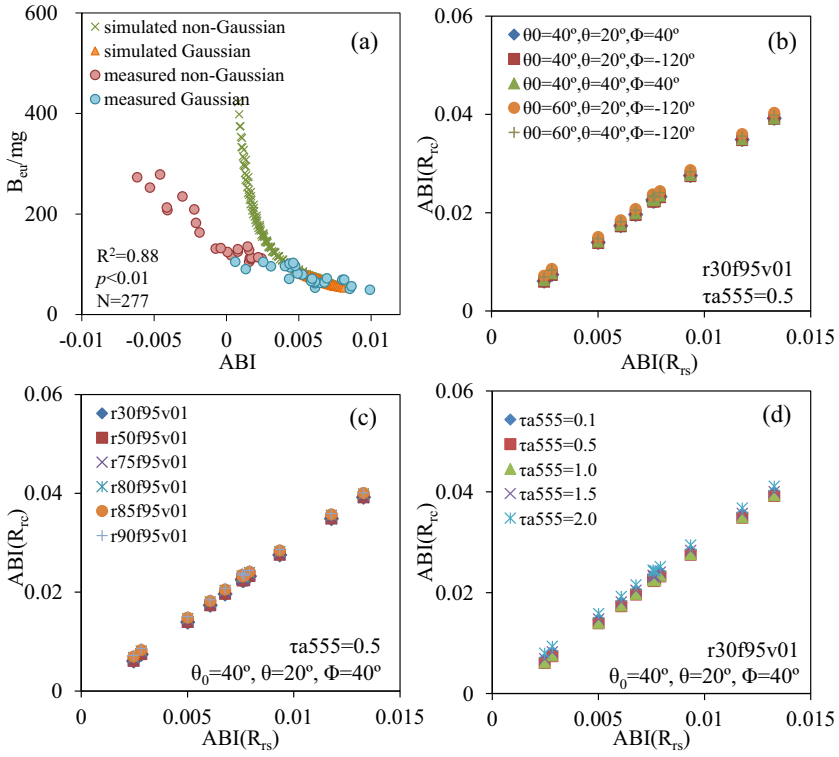

Fig. 3. (a) Relationship between ABI and B_{eu} based on simulated and measured data and between R_{rs}-based ABI and R_{rc}-based ABI under: (b) different angles of observation for $\tau a555 = 0.5$, aerosol type r30f95v01; (c) different aerosol types with SeaDAS LUT for $\tau a555 = 0.5, \theta_0 = 40°; \theta = 20°; \Phi = 40°$; (d) different optical thicknesses for aerosol type r30f95v01, $\theta_0 = 40°; \theta = 20°; \Phi = 40°$.

relationship (*SI Appendix*, Table. S4) and an exponential model (Eq. (15)) was finally used ($R^2 = 0.89, p < 0.01, N = 50$) to describe the relationship. This fitting model was based on an assumption that water depth is 3 m. Therefore, B_{ou} in water column is calculated by multiplying mean Chl-a concentration by the water depth outside euphotic layer as:

$$B_{ou} = 79.68 \times \exp(-0.005 \times B_{eu})/(3-Z_{eu}) \times (D-Z_{eu}) \quad (15)$$

where D represents water depth (m) of the specific location.

3.2. Synchronous validation

The estimation of algal biomass was validated using field data of R_{rs} and measured algal biomass. The result showed a significant correlation ($R^2 = 0.78, p < 0.01, N = 52$, *SI Appendix*, Fig. S4a). RMSE of B_{eu} and B_{ou} based on R_{rs} were 14.46 mg (MRE = 22.03%, $N = 52$) and 11.38 mg (MRE = 21.50%, $N = 52$) separately.

The model was then applied on synchronous satellite data and validated using in situ data. The relationship between R_{rc}-based simulated result and in situ biomass shows an acceptable precision for estimation (*SI Appendix*, Fig. S4b) with MRE = 21.86% and RMSE = 17.98 mg. The possible reasons of errors of the algal biomass could be: (1) the sampling time of the field experiment differs during the passing time of satellite (i.e. the crossing times of 10:30 a.m. and 1:30 p.m. in one day); (2) algae of Lake Chaohu is affected by external factors such as wind speed and water flow, or other optically active substances(i.e. turbidity); (3) scale differences between field data and satellite data; (4) complex conversion relationship between R_{rs} and R_{rc}.

3.3. Inter-day and consecutive days validation

The stability of ABI algorithm in different hours of the same day and in consecutive days were further explored. Algal biomass of the entire lake was estimated based on Terra and Aqua separately in the same day of 2014. The scatter plot (*SI Appendix*, Fig. S4c) showed relationships between Terra-based algal biomass and Aqua-based algal biomass with high correlation ($R^2 = 0.87$, $p < 0.01$, $N = 61$) and low bias (RMSE = 3.65 t, MRE = 3.5%), which proved the stability of the algorithm.

Values of algal biomass at the corresponding pixels from Aqua and Terra were also compared to test the temporal consistency of algal biomass estimates. The total algal biomass of Lake Chaohu estimated by MODIS Terra and Aqua R_{rc} data in different seasons (January 21, March 17, May 6 and September 30, 2014) showed no obvious fluctuation in one day (Fig. 4). For example, the algal biomass on September 30 calculated from MODIS Terra and Aqua were 69.12 t and 69.01 t, respectively, with a change rate of −0.15% (Fig. 4(a), (b)). However, scatter plots showed that 3.93% differences of algal biomass at the same pixel were more than 30% and 1.27% of that more than 50%, which arises the variation in spatial distribution (Fig. 4(c)). This is because the spatial distribution of algal biomass changed greatly in a day under the influence of wind and water disturbance. Spatial characteristics of the algal biomass in different seasons (Fig. 4(a), (b), (d), (e), (g), (h), (j), (k)) also confirmed the previous research on algae species of Lake Chaohu (Zhang et al. 2016).

The area of algal bloom and total algal biomass in whole lake based on MODIS R_{rc} data in several consecutive days (21st of July to 24th of July 2011) were compared (*SI Appendix*, Fig. S5, Table. S5). The result shows that the area of algal bloom decreased from 477.93km^2 to 11.08km^2 for three consecutive days, with a change rate of −97.68%. However, the algal biomass in the whole lake only changed from 87.05 t to 85.92 t. The occurrence of algal blooms happened in the vertical direction of water, the change in the algal biomass is not the main reason that causes the large area of bloom (Xue et al. 2015). Statistics of the algal biomass in consistent days also showed the robust algorithm.

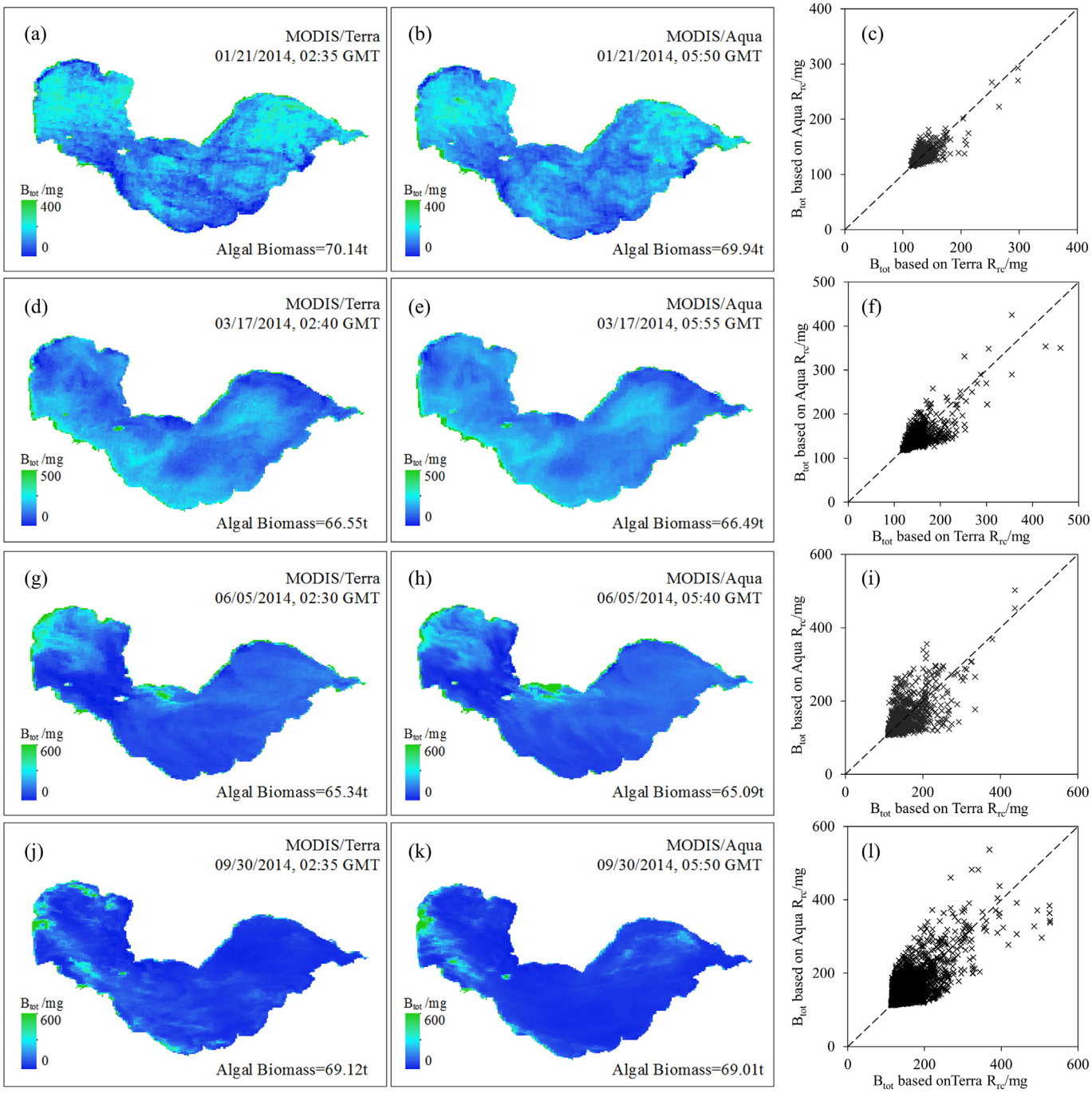

Fig. 4. Algal biomass in Lake Choahu calculated by MODIS Terra and Aqua Rrc in: (a) and (b)January; (d) and(e) March; (g) and (h) June; (j) and (k) September, and comparison of algal biomass at the same pixel(c), (f), (i), (l).

3.4. Algal biomass trend analysis

Statistical results of monthly average algal biomass estimates (*SI Appendix*, Fig. S6a) showed seasonal variation of algal biomass in Lake Chaohu, with two peaks that occurred in February and August respectively. Compared with the estimation of long-term column-integrated algal biomass in Lake Chaohu (Li et al. 2017), this study made up results in July, August, and September under the conditions of frequent surface algal blooms that were not discussed in Li's study. The annual average algal biomass estimates from 2012 to 2017 (*SI Appendix*, Fig. S6b) indicated that the algal biomass in Lake Chaohu was relatively stable from 2012 to 2014 and became higher during the period from 2015 to 2017. The spatial variation of B_{tot} in Lake Chaohu from 2012 to 2017 showed more obvious change in the western lake than that of in eastern lake (Fig. 5).

3.5. Sensitivity analysis

Absorption coefficients of phytoplankton, non-algal particulates (NAP), and colored dissolved organic matter (CDOM), which make up optically active constituents (OACs), are important to optical variability of natural waters and apparent optical properties (AOPs) (Bricaud et al., 2012). ABI based on the Ecolight Gauss simulation under different a_g (440) (0.35–1.35 m^{-1} with every 0.25 m^{-1} where SPIM =

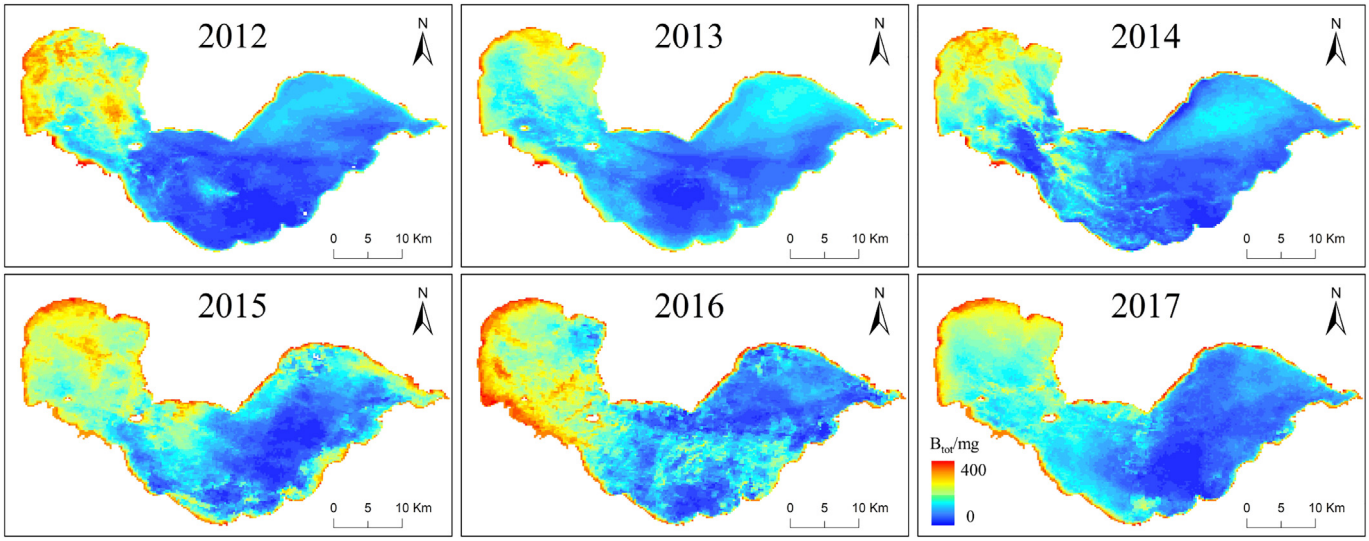

Fig. 5. Spatial distribution of B_{tot} in Lake Chaohu from 2012 to 2017.

30 mg·L^{-1}) and SPIM concentrations(20–80 mg·L^{-1} with every 10 mg·L^{-1} where $a_g(440) = 0.85$ m^{-1}) were compared to explore the sensitivity of algorithm. Fig. 6(a) showed that when $a_g(440)$ changed from 0.35 m^{-1} to 1.10 m^{-1}, relative error of ABI changed from 0.00597 to 0.00607, which showed only a 0.6% growth. Previous study has confirmed that the contribution of CDOM absorption was lower than 30%, which illustrated that phytoplankton and NAP were the primary sources of spatial and vertical variability in absorption properties (Xue et al. 2017). Relative errors of ABI with different change rates of SPIM were further compared. As shown in Fig. 6(b), when the change rate of SPIM is 10%, 50% and 100%, the corresponding relative errors of ABI is 6.94%, 28.19% and 54.75%, respectively. As SPIM changes under 50%, the relative error of ABI changes under 30%. The larger the change rate of SPIM, the more drastic the change of relative error of ABI. Extreme SPIM variations were considered as the change rates of SPIM concentration at the same location generally will not vary drastically (<50%). Therefore, variations of $a_g(440)$ has less effect on ABI but more sensitive to changes in SPIM concentration. Therefore, Turbid Water Index (TWI) (Liang et al. 2017) was suggested to remove high turbidity waters and avoid underestimation by MODIS that caused by the high SPIM in these samplings.

The RGB and ABI images of MODIS dataset were visually compared, together with spectral analysis and histogram statistics, to evaluate how the ABI algorithm performed under thin clouds conditions. The study illustrated two RGB images (Red = Band 1, Green = Band 4, Blue = Band 3) on October 28, 2014 based on Terra and Aqua respectively, with no cloud Fig. 7(a) and thin clouds Fig. 7(b) in western lake. It was found that the ABI values derived under thin clouds condition at 03:05 GMT (Fig. 7(c)) were similar to those derived under no cloud conditions at 05:25 GMT of the same day (Fig. 7(d)). Four points were selected to obtain the spectral curve under different cloud cover conditions (Fig. 7(a), (b)). Points 1 and 3 show blooms at the same locations, which we call it "bloom water", while points 2 and 4 show turbidity water. Despite the significantly different R_{rc} spectra collected in similar location but under different cloud cover conditions (Fig. 7(e)), the ABI values from both images were similar by histogram statistics (Fig. 7(f)). The mean ABI value change by only 2.8%, indicating tolerance of the ABI algorithm to thin clouds condition.

4. Discussion

4.1. Comparison with previous study

Previous study has estimated the algal biomass in Lake Chaohu using an empirical algorithm that built the relationship between Chl-a on the surface and vertical Chl-a concentrations (Li et al. 2017). The

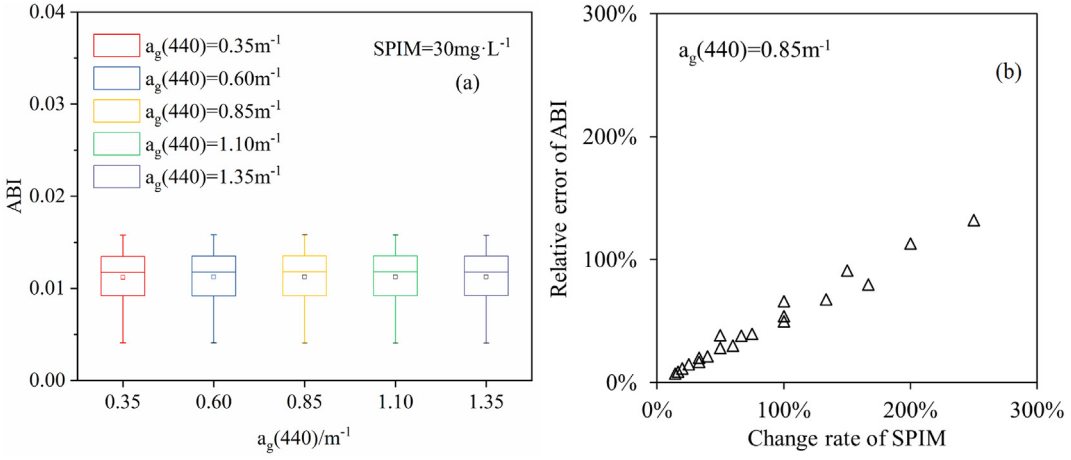

Fig. 6. ABI values at different $a_g(440)$ (0.35,0.60,0.85,1.10,1.35 m^{-1}) with SPIM = 30 mg·L^{-1} and (b) relative errors of ABI with different change rates of SPIM under $a_g(440) = 0.85$ m^{-1}.

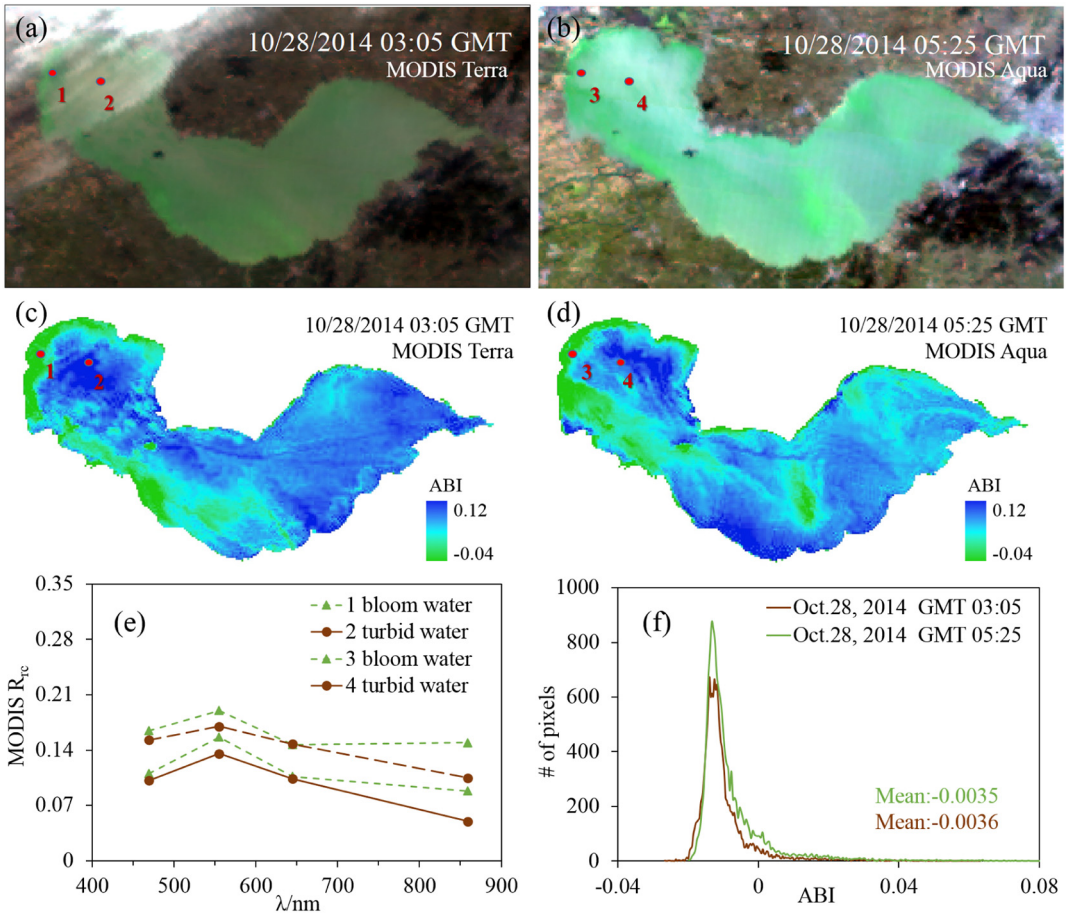

Fig. 7. Robust of the ABI under different cloud conditions. (a) and (c) show MODIS RGB and ABI images for GMT 03:05 on Oct 28, 2014, while (b) and (d) show MODIS RGB and ABI images for GMT 05:25 on the same day. The R_{rc} spectra from 4 locations are extracted and shown in (e). Point 1 and 3 show blooms at the same locations, while point 2 and 4 show turbid water locations. Histograms in (f) show the ABI distribution statistics in the whole lake, which covers both no cloud and thin clouds regions.

verification results prove the applicability and reliability of the algorithm in Lake Chaohu (MRE = 22.2%). In the present study, the ABI algorithm was validated using the same dataset with synchronous satellite data (*SI Appendix*, Fig. S7). The result showed a good correlation between the measured biomass and the estimated biomass ($R^2 = 0.95$, $N = 106$, RMSE = 8.3 mg, MRE = 5.5%). Compared with the existing algorithm, MRE of the proposed algorithm reduced from 22.2% to 5.5%, indicating better performance. In the interval with a high total amount of algae, the algal biomass calculated using the proposed algorithm was more accurate than that calculated using the original algorithm.

4.2. Possible application for OLCI

The R_{rc} data of OLCI in Lake Chaohu on February 26, 2017 was used in the study. ABI was constructed using visible and near infrared band (443, 560, 665, and 865 nm), and compared with the ABI based on MODIS on the same day. Fig. 8(a) and (b) are RGB images of OLCI and MODIS satellite data (OLCI: Red = Oa8, Green = Oa6, Blue = Oa3; MODIS: Red = Band 1, Green = Band 4, Blue = Band 3). The corresponding OLCI-based ABI, which showed in Fig. 8(c) was generally the same as MODIS-based ABI (Fig. 8(d)) in spatial distribution. Histograms in Fig. 8(e) show distribution statistics performed on the ABI. The average value of ABI based on OLCI is 0.0064 ± 0.0081, and the average value of ABI based on MODIS is 0.0068 ± 0.0083. 60 samples were further arranged throughout the whole lake to compare the difference of ABI between OLCI and MODIS data. Line charts of Fig. 8(f) showed a good accuracy with RMSE = 0.0026 and MRE = 11.93%. Reasons for the error may be: (1) Different passing time of MODIS and OLCI; (2) Different sensor performances (signal-to-noise ratio, radiation resolution, spatial resolution, etc.). However, ABI algorithm still indicates the potential ability to retrieve algal biomass using OLCI data, but coefficients need to be adjusted in combination with the measured data.

5. Conclusion

A novel algorithm was put forward to facilitate the hard work in estimating the algal biomass in eutrophic lakes by considering vertically heterogeneous distribution of chlorophyll. Applying baseline subtraction, ABI algorithm dramatically counteracts disturbance from difference in observation conditions, aerosol types and thickness, thus implements conversion from ground R_{rs} data to satellite R_{rc} data. Performance of ABI under circumstance of thin clouds and different $a_g(440)$ make it possible to the further long-term observation and calculation of algal biomass distribution in Lake Chaohu (2012–2017), which was essential for growth of algae and eutrophication treatment. Promising application was found when applying ABI algorithm to OLCI, thus increase the possibilities to provide substitution for MODIS data. So far, this research represents a case study for Lake Chaohu and we believe the algorithm can be extended to other eutrophic lakes when specific parameters are modified and verified by field data and consistency checks.

CRediT authorship contribution statement

Minqi Hu: Conceptualization, Methodology, Writing – original draft, Writing – review & editing. **Yuchao Zhang:** Conceptualization,

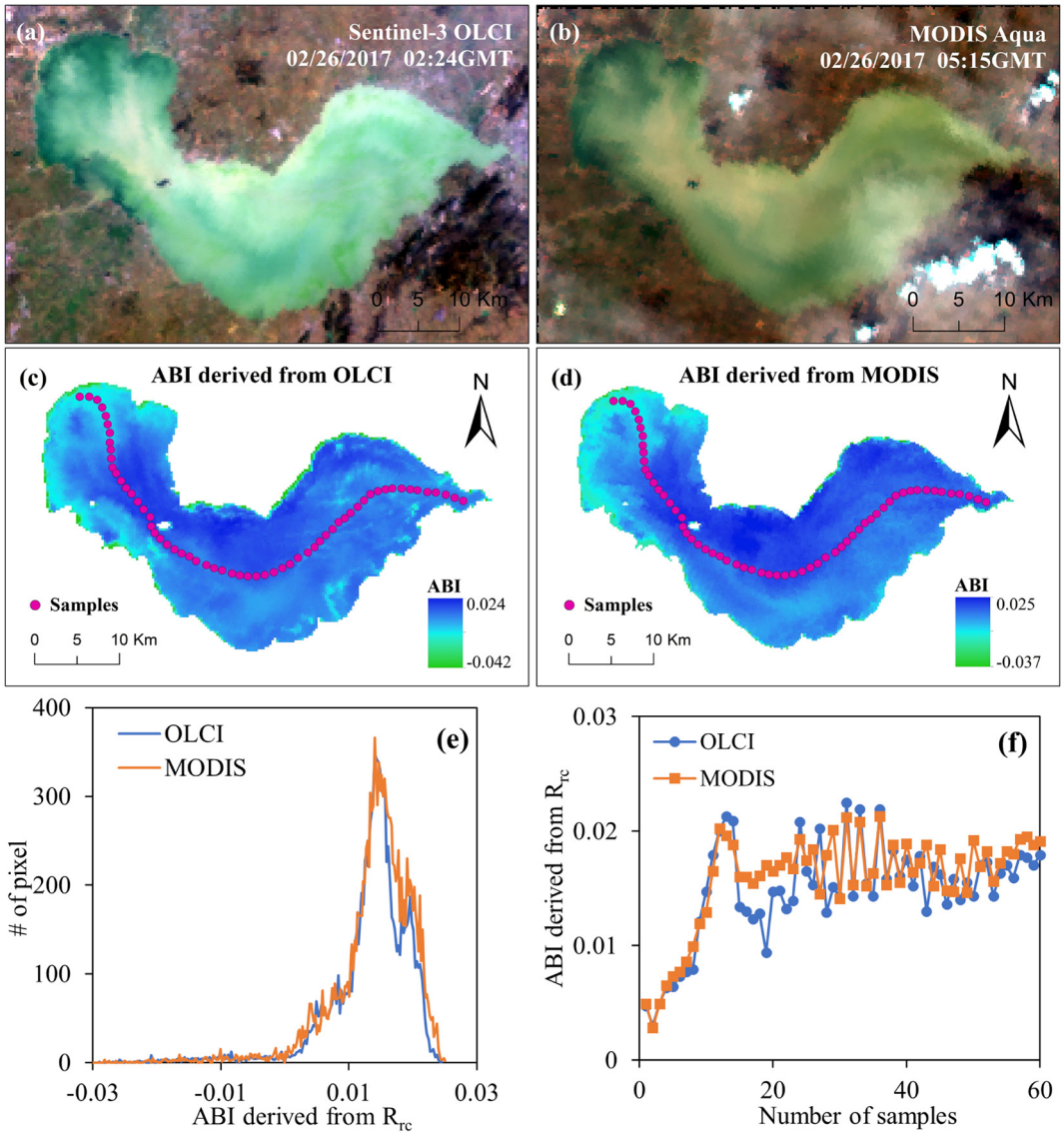

Fig. 8. Application of the algorithm to OLCI. (a), (b) OLCI and MODIS RGB image for 26th of February on 2017; (c), (d) OLCI and MODIS ABI imagery; (e) histogram statistics of the ABI distributions from two remote sensors; (f) Values of ABI based on OLCI and MODIS at different samples.

Supervision, Writing – review & editing. **Ronghua Ma:** Supervision, Investigation, Resources. **Kun Xue:** Methodology, Writing – review & editing, Resources, Investigation. **Zhigang Cao:** Data curation, Resources, Investigation. **Qiao Chu:** Writing – review & editing, Investigation. **Yuanyuan Jing:** Resources, Investigation.

Declaration of competing interest

The authors declare that they have no known competing financial interests or personal relationships that could have appeared to influence the work reported in this paper.

Acknowledgment

This work was funded by the National Natural Science Foundation of China (Grant No. 41671371), Jiangsu Provincial Key Research and Development Program (BE2019774) and the Scientific Instrument Developing Project of the Chinese Academy of Sciences (Grant No. YJKYYQ20200048). Field data were provided by the Scientific Data Sharing Platform for Lake and Watershed, Nanjing Institute of Geography and Limnology, Chinese Academy of Sciences. DEM data was supported from Lake-Watershed Science Data Center, National Earth System Science Data Sharing Infrastructure, National Science & Technology Infrastructure of China (http://lake.geodata.cn).

Appendix A. Supplementary data

Supplementary data to this article can be found online at https://doi.org/10.1016/j.scitotenv.2020.144811.

References

Bi, Sh., Li, Y., Lv, H., Zhu, L., Mu, M., Lei, S., Xu, J., Wen, Sh., Ding, X., 2018. Estimation of chlorophyll-a concentration in Lake Erhai based on OLCI data. Journal of Lake Science 30, 701–712.

Binding, C., Jerome, J., Bukata, R., Booty, W., 2008. Spectral absorption properties of dissolved and particulate matter in Lake Erie. Remote Sens. Environ. 112, 1702–1711.

Bricaud, A., Ciotti, A.M., Gentili, B., 2012. Spatial-temporal variations in phytoplankton size and colored detrital matter absorption at global and regional scales, as derived from twelve years of SeaWiFS data (1998–2009). Glob. Biogeochem. Cycles 26, 262–269.

Cao, H., Kong, F., Luo, L., Shi, X., Yang, Z., Zhang, X., Tao, Y., 2006. Effects of wind and wind-induced waves on vertical phytoplankton distribution and surface blooms of Microcystis aeruginosa in Lake Taihu. J. Freshw. Ecol. 21, 231–238.
Cao, Z., Duan, H., Feng, L., Ma, R., Xue, K., 2017. Climate- and human-induced changes in suspended particulate matter over Lake Hongze on short and long timescales. Remote Sens. Environ. 192, 98–113.
Carlson, R., 1977. A trophic state index for lakes. Limnology and Oceanography - Limnology and Oceanography 22, 361–369.
Chen, X., Yang, X., Dong, X., Liu, E., 2013. Environmental changes in Chaohu Lake (southeast, China) since the mid-20th century: the interactive impacts of nutrients, hydrology and climate. Limnologica - Ecology and Management of Inland Waters 43, 10–17.
Duan, H., Zhang, S., Zhang, Y., 2008. Cyanobacteria bloom monitoring with remote sensing in Lake Taihu. Journal of Lake Science 20, 145–152.
Feng, L., Hu, C., Chen, X., Tian, L., Chen, L., 2012. Human induced turbidity changes in Poyang Lake between 2000 and 2010: observations from MODIS. Journal of Geophysical Research Oceans 117, C07006.
Frolov, S., Ryan, J., Chavez, F., 2012. Predicting euphotic-depth-integrated chlorophyll-a from discrete-depth and satellite-observable chlorophyll-a off central California. Journal of Geophysical Research Oceans 117, 247–253.
Gordon, H., McCluney, W., 1975. Estimation of the depth of sunlight penetration in the sea for remote sensing. Appl. Opt. 14, 413–416.
Hu, C., 2009. A novel ocean color index to detect floating algae in the global oceans. Remote Sens. Environ. 113, 2118–2129.
Hu, C., Chen, Z., Clayton, T., Swarzenski, P., Brock, J., Muller–Karger, F., 2004. Assessment of estuarine water-quality indicators using MODIS medium-resolution bands: initial results from Tampa Bay, FL. Remote Sens. Environ. 93, 423–441.
Hu, C., Lee, Z., Franz, B., 2011. Chlorophyll-a algorithms for oligotrophic oceans: a novel approach based on three-band reflectance difference. Journal of Geophysical Research Oceans 117, C01001.
Hu, M., Zhang, Y., Ma, R., Zhang, Y., 2018. Spatial and temporal dynamics of floating algae blooms of Lake Chaohu in 2016 and environmental drivers. Environmental Science. 039, 4925–4937.
Jiang, Y., He, W., Liu, W., Qin, N., Ouyang, H., Wang, Q., Kong, X., He, Q., Yang, C., Yang, B., Xu, F., 2014. The seasonal and spatial variations of phytoplankton community and their correlation with environmental factors in a large eutrophic Chinese lake (Lake Chaohu). Ecol. Indic. 40, 58–67.
Kahru, M., 1994. Satellite detection of increased cyanobacteria blooms in the Baltic Sea: natural fluctuation or ecosystem change? Ambio 23, 469–472.
Kirk, J., 1994. Light and photosynthesis in aquatic ecosystems. J. Ecol. 45.
Kong, F., Gao, G., 2005. Hypothesis on cyanobacteria bloom-forming mechanism in large shallow eutrophic lakes. Acta Ecol. Sin. 25, 589–595.
Kutser, T., Metsamaa, L., Strömbeck, N., Vahtmäe, E., 2006. Monitoring cyanobacterial blooms by satellite remote sensing. Estuarine Coastal & Shelf Science 67, 303–312.
Le, C., Li, Y., Zha, Y., 2008. Eutrophic depth: retrieval from in situ reflectance and application in assessing eutiophication. Acta Ecol. Sin. 28 (6), 2614–2621.
Le, C., Hu, C., English, D., Cannizzaro, J., Kovach, C., 2013. Climate-driven chlorophyll-a changes in a turbid estuary: observations from satellites and implications for management. Remote Sens. Environ. 130, 11–24.
Lee, Z., Jiang, M., Davis, C., Pahlevan, N., Ahn, Y., Ma, R., 2012. Impact of multiple satellite ocean color samplings in a day on assessing phytoplankton dynamics. Ocean Science Journal 47, 323–329.
Lei, S., Xu, J., Li, Y., Du, C., Li, L., 2020a. An approach for retrieval of horizontal and vertical distribution of total suspended matter concentration from GOCI data over Lake Hongze. Sci. Total Environ. 700, 134524.
Lei, S., Xu, J., Li, Y., Lyu, H., Liu, G., Zheng, Z., Xu, Y., Du, C., Zeng, S., Wang, H., Dong, X., Cai, X., Li, J., 2020b. Temporal and spatial distribution of Kd(490) and its response to precipitation and wind in lake Hongze based on MODIS data. Ecol. Indic. 108, 105684.
Li, W., Ji, G., Yang, J., 1995. Estimation Cyanophyta Biomass Standing Crops in Meiliang Gulf of Lake Taihu by Satellite Remote Sensing. 2 pp. 23–28.
Li, J., Zhang, Y., Ma, R., Duan, H., Loiselle, S., Xue, K., Liang, Q., 2017. Satellite-based estimation of column-integrated algal biomass in nonalgae bloom conditions: a case study of Lake Chaohu, China. IEEE Journal of Selected Topics in Applied Earth Observations and Remote Sensing 10, 450–462.
Li, J., Ma, R., Xue, K., Zhang, Y., Loiselle, S., 2018. A remote sensing algorithm of column-integrated algal biomass covering algal bloom conditions in a shallow eutrophic lake. ISPRS International Journal of Geo-Information 7.
Liang, P., Wang, H., Ma, F., 2013. Effect of hydrodynamic conditions on water eutrophication: a review. J. Lake Sci. 25 (4), 455–462.
Liang, Q., Zhang, Y., Ma, R., Loiselle, S., Li, J., Hu, M., 2017. A MODIS-based novel method to distinguish surface cyanobacterial scums and aquatic macrophytes in Lake Taihu. Remote Sens. 9, 133.
Liu, J., Wan, J., 2018. Monitoring cyanobacteria blooms in East Lake using HJ-1 multispectral satellite images. Advances in Meteorological Science and Technology 5, 91–95.
Lodhi, M., Rundquist, D., 2001. A spectral analysis of bottom-induced variation in the colour of Sand Hills lakes, Nebraska, USA. Int. J. Remote Sens. 22, 1665–1682.
Lwjr, H., Itsweire, E., Esaias, W., 1992. Determination of phytoplankton chlorophyll concentrations in the Chesapeake Bay with aircraft remote sensing. Remote Sens. Environ. 40, 79–100.
Ma, R., Tang, J., Dai, J., 2006. Bio-optical model with optimal parameter suitable for Taihu Lake in water colour remote sensing. Int. J. Remote Sens. 27, 4305–4328.
Ma, R., Duan, H., Liu, Q., & Loiselle, S. (2011a). Approximate bottom contribution to remote sensing reflectance in Taihu Lake, China. *Journal of Great Lakes Research*. 37, 0–25.
Ma, R., Jiang, G., Duan, H., Bracchini, L., Loiselle, S., 2011b. Effective upwelling irradiance depths in turbid waters: a spectral analysis of origins and fate. Optical Express. 19, 7127–7138.
Ma, M., Zhang, Y., Qian, X., Ma,R., & Duan, H. (2014). Influence of algae vertical profiles on chlorophyll-a retrieval algorithm in inland lakes: Hydrolight simulation. J. Infrared Millim Waves. 33, 666–673.
Matthews, M., Bernard, S., Robertson, L., 2012. An algorithm for detecting trophic status (chlorophyll-a), cyanobacterial-dominance, surface scums and floating vegetation in inland and coastal waters. Remote Sens. Environ. 124, 637–652.
Mentaschi, L., Besio, G., Cassola, F., Mazzino, A., 2013. Problems in RMSE-based wave model validations. Ocean Model. 72, 53–58.
Miller, R., Mckee, B., 2004. Using MODIS Terra 250 m imagery to map concentrations of total suspended matter in coastal waters. Remote Sens. Environ. 93, 259–266.
Mobley, C.D., 1994. Light and Ware: Radiative Transfer in Natural Waters. Academic Press.
Mobley, C.D., 1999. Estimation of the remote-sensing reflectance from above-surface measurements. Appl. Opt. 38 (36), 7442–7455.
Mobley, C.D., Sundman, L.K., 2008. Hydrolight 5. Ecolight5 User Guide.
Morel, A., Berthon, J., 1989. Surface pigments, algal biomass profiles, and potential production of the euphotic layer: relationships reinvestigated in view of remote-sensing applications. Limnology & Oceanography 34, 1545–1562.
Mueller, J., Fargion, G., McClain, C., Pegau, W., Zaneveld, J., Mitchell, B., Kahru, M., Wieland, J., Stramska, M., 2003. Ocean Optics Protocols for Satellite Ocean Color Sensor Validation Revision 3, V. 2.
Oliver, R., Ganf, G., 2007. Freshwater Blooms. Kluwer Academic Publishers.
Petus, C., Chust, G., Gohin, F., Doxaran, D., Froidefond, J., Sagarminaga, Y., 2010. Estimating turbidity and total suspended matter in the Adour River plume (South Bay of Biscay) using MODIS 250-m imagery. Cont. Shelf Res. 30, 379–392.
Safonov, M.G., Chiang, R.Y., 1988. Model reduction for robust control: a schur relative error method. International Journal of Adaptive Control and Signal Processing 2, 259–272.
Serôdio, J., Cartaxana, P., Coelho, H., Vieira, S., 2009. Effects of chlorophyll fluorescence on the estimation of microphytobenthos biomass using spectral reflectance indices. Remote Sens. Environ. 113, 1760–1768.
Shanmugam, P., Suresh, M., Sundarabalan, B., 2013. OSABT: an innovative algorithm to detect and characterize ocean surface algal blooms. IEEE Journal of Selected Topics in Applied Earth Observations & Remote Sensing 6, 1879–1892.
Shi, K., Zhang, Y., Liu, X., Wang, M., Qin, B., 2014. Remote sensing of diffuse attenuation coefficient of photosynthetically active radiation in Lake Taihu using MERIS data. Remote Sens. Environ. 140, 365–377.
Shi, Z., Zhang, Y., Cai, T., 2015. Determination of the spectral absorption coefficients of suspended particulate matters in the shallow lakes in the middle and lower reaches of Yangtze River. Journal of Lake Science. 27, 519–526.
Silulwane, N., Richardson, A., Shillington, F., Mitchell-Innes, B., 2001. Identification and classification of vertical chlorophyll patterns in the Benguela upwelling system and Angola-Benguela front using an artificial neural network. S. Afr. J. Mar. Sci. 23, 37–51.
Tang, J., Xue, Y., Yu, T., Guan, Y., 2005. Aerosol optical thickness determination by exploiting the synergy of TERRA and AQUA MODIS. Remote Sens. Environ. 94, 327–334.
Tang, J., Shi, T., Wu, X., Cao, H., Li, X., Hua, R., Tang, F., Yue, Y., 2015. The occurrence and distribution of antibiotics in Lake Chaohu, China: seasonal variation, potential source and risk assessment. Chemosphere 122, 154–161.
Uitz, J., Claustre, H., Morel, A., Hooker, S., 2006. Vertical distribution of phytoplankton communities in open ocean: an assessment based on surface chlorophyll. Journal of Geophysical Research Oceans 111.
Wang, X., Xi, B., Huo, S., Deng, L., Pan, H., Xia, X., Zhang, J., Ren, Y., Liu, H., 2013. Polybrominated diphenyl ethers occurrence in major inflowing rivers of Lake Chaohu (China): characteristics, potential sources and inputs to lake. Chemosphere 93, 1624–1631.
Wang, X., Zhang, M., Yin, J., 2018. Composition and influential factors of phytoplankton function groups in Lake Chaohu. Journal of Lake Science 30, 431–440.
Xi, S., Zhou, C., Liu, G., Wu, L., Wang, P., 2016. Spatial and temporal distributions of nitrogen and phosphate in the Chaohu Lake. Environmental Science. 37, 542–547.
Xue, K., Zhang, Y., Duan, H., Ma, R., Steven, L., Zhang, M., 2015. A remote sensing approach to estimate vertical profile classes of phytoplankton in a eutrophic Lake. Remote Sens. 86, 14403–14427.
Xue, K., Zhang, Y., Duan, H., Ma, R., 2016. Variability of light absorption properties in optically complex inland waters of Lake Chaohu, China. J. Great Lakes Res. 43, 17–31.
Xue, K., Zhang, Y., Ma, R., 2017. An approach to correct the effects of phytoplankton vertical nonuniform distribution on remote sensing reflectance of cyanobacterial bloom waters. Limnology & Oceanography Methods 15 (3).
Zaneveld, J.R., Barnard, A., Boss, E., 2005. Theoretical derivation of the depth average of remotely sensed optical parameters. Opt. Express 13, 9052–9061.
Zhang, Y., Liu, X., Yin, Y., Wang, M., Qin, B., 2012. A simple optical model to estimate diffuse attenuation coefficient of photosynthetically active radiation in an extremely turbid lake from surface reflectance. Opt. Express 20, 20482–20493.
Zhang, Y., Ma, R., Duan, H., Loiselle, S.A., Xu, J., Ma, M., 2014. A novel algorithm to estimate algal bloom coverage to subpixel resolution in Lake Taihu. IEEE Journal of Selected Topics in Applied Earth Observations & Remote Sensing 7, 3060–3068.
Zhang, Y., Ma, R., Zhang, M., Duan, H., Steven, L., Xu, J., 2015. Fourteen-year record (2000−2013) of the spatial and temporal dynamics of floating algae blooms in Lake Chaohu, observed from time series of MODIS images. Remote Sens. 7, 10523–10542.
Zhang, M., Zhang, Y., Yang, Z., Wei, L., Yang, W., Chen, C., Kong, F., 2016. Spatial and seasonal shifts in bloom-forming cyanobacteria in Lake Chaohu: patterns and driving factors. Phycol. Res. 64, 44–55.